J. Fluid Mech. (1983), *vol.* 132, *pp.* 87–103
Printed in Great Britain

Scaling of the bursting frequency in turbulent boundary layers

By R. F. BLACKWELDER AND J. H. HARITONIDIS†
Department of Aerospace Engineering, University of Southern California, Los Angeles, California

(Received 17 August 1981 and in revised form 13 October 1982)

The bursting frequency in turbulent boundary layers has been measured over the Reynolds-number range $10^3 < U_\infty \theta/\nu < 10^4$. When scaled with the variables appropriate for the wall region, the non-dimensional frequency was constant independent of Reynolds number. A strong effect of the sensor size was noted on the measured bursting frequency. Only sensors having a spatial scale less than twenty viscous lengthscales were free from spatial-averaging effects and yielded consistent results. The spatial-resolution problem was apparently the reason for erroneous results reported in the past.

1. Introduction

Within the last decade, many of the attributes of turbulent shear flows have been ascribed to large coherent eddy structures. In bounded shear flows there appeared to be two distinct coherent eddies; one governs the outer flow field and is responsible for entertainment in the case of turbulent boundary layers, and the second controls the wall region near the boundary. The wall region appears to be dominated by the bursting phenomenon, which consists of several distinct characteristics. In this region the flow seems to have a propensity to form ubiquitous streamwise vortices having radii typically between $20\nu/u_\tau$ and $50\nu/u_\tau$. They appear in counter-rotating pairs, as has been deduced by Bakewell & Lumley (1967) from streamwise velocity correlations. Although their streamwise extent is presently unknown, it is probably at least an order of magnitude greater than their diameter. Brown & Thomas (1977), Coles (1979) and others have suggested that these vortices are consistent with a Taylor–Görtler instability; however, at present their generation mechanism is still unknown.

One of the more easily visualized aspects of the bursting phenomenon is the presence of streaks of low-speed fluid. They seem to form between two of the vortices as they remove low-speed fluid from the wall and lift it upward as suggested by Blackwelder (1979). These streaks are typically 10–$20\nu/u_\tau$ wide and 100–$1000\nu/u_\tau$ long, and appear randomly in space and time. Kline *et al.* (1967) suggested that the streaks usually end by being lifted away from the wall. At about the same time and/or slightly thereafter, they appear to oscillate. This oscillatory motion increases in amplitude and scale until a breakdown occurs, at which time completely chaotic motion ensues. This phase of the wall structure occurs on a very short timescale, and consequently has been called the 'burst'. Corino & Brodkey (1969) showed that, soon

† Present address: Massachusetts Institute of Technology, Dept of Aeronautics and Astronautics, 37–461, Cambridge, MA 02139.

thereafter, a larger-scale motion emanating from the outer flow field approaches the wall and cleans the entire area of the chaotic motion; consequently, this phase of the structure has been called a 'sweep'. The sweep seems to scale with the outer flow variables, i.e. δ and U_∞, and it appears to form a highly irregular interface with the wall region. The irregularities on this interface appear to scale with the wall variables ν and u_τ. These irregularities have been called 'pockets' by Falco (1980), and have a scale of approximately $100\nu/u_\tau$.

The different phases and aspects of the bursting phenomena have been obtained by many different experimental techniques, which can be broadly classified as visualization and probe methods. Both types of experiments have their relative advantages and disadvantages; however, no single method or combination of techniques has been able to study the entire structure as outlined above. The visualization techniques have used dye, hydrogen bubbles, and particles to illuminate different aspects of the bursting phenomena. Because of the small scales of the bursting phenomena, the only probes that have been used to study this eddy structure have been hot-wire and hot-film anemometers and pinhole pressure transducers.

Most of the studies have used different algorithms and techniques to detect the bursting phenomena. In spite of these differences, the spatial configuration and scales of the wall structure are generally agreed upon by the different investigators, as evidenced by the discussions included in the Lehigh Symposium on Turbulent Boundary Layers (Smith & Abbott 1979). However, there is considerable disagreement concerning the frequency of occurrence and the scaling of the bursting structure in bounded turbulent shear flows. The research reported here attempts to resolve this disagreement. The lack of agreement is most frequently ascribed to the different detection techniques utilized. Rao, Narasimha & Badri Narayanan (1971) attempted to determine how the bursting frequency varied as the Reynolds number changed. They devised a detection criterion using differentiation and simple filtering together with a threshold level. Although their mean bursting rate was highly sensitive to the threshold discriminator setting, they concluded that the mean frequency scaled with the outer flow variables δ and U_∞ over a Reynolds-number range $600 < U_\infty\theta/\nu < 9000$. On the other hand, it is particularly interesting to note that, when different techniques were used over small ranges of Reynolds number as shown in their figure 9, there is a tendency for the mean period to decrease as the Reynolds number increases, e.g. the data of Schraub & Kline (1965), Laufer & Badri Narayanan (1971) and Kim, Kline & Reynolds (1971). The present investigation was inspired in part by a comparison between the work of Blackwelder & Kaplan (1976) and Blackwelder & Eckelmann (1978). Both investigations utilized the same burst-detection criteria and obtained the same conditional averages of the wall-layer structure. However, the frequency of occurrence of the bursting process could not be matched by scaling with the outer flow variables.

To study the bursting frequency and determine its scaling and variation over a Reynolds-number range, several parameters must be considered. First, the flow field must be chosen: i.e. a boundary-layer, pipe or channel flow. Even though there are great similarities between the structure of the bursting phenomenon between these different flow fields, it can be argued that if the bursting frequency scales with the outer flow variables then the frequencies may be different between these flow fields because their outer flow fields are indeed different. Secondly, the origin and development of the flow field should be considered. For example, in a boundary layer the turbulence may be naturally occurring or it may have its origin at a trip. Thirdly, the type of sensor to be used will most undoubtedly influence the number of bursts

detected per unit time. Even though probe techniques will yield more-reproducible results from one laboratory to another, some care must be taken to ensure that the probes have the same spatial resolution, frequency response, etc. Fourthly, the best location in the wall region for detecting the bursting structure must be determined. Lastly, the detection criterion itself is probably the largest variable in determining the mean bursting frequency. Many different techniques have been utilized, and most of the scatter in the resulting data can probably be attributed to the different detection methods. Other parameters can also be identified; however, those above seem to be the most important ones.

The present research was designed to study the dependence of the bursting frequency upon the Reynolds number and to explain some of the discrepancies reported in the literature. From the beginning, it was decided to use probe techniques to provide better reproducibility as the Reynolds number and other parameters were varied. Consequently, the detection scheme must be a circuit or a digital algorithm having the ability to respond to the different frequency ranges encountered over the entire Reynolds-number range. Since the short-time averaging technique has been used by the broadest number of researchers (including Blackwelder & Kaplan 1972, 1976; Zakkay, Barra & Wang 1978; Zakkay, Barra & Hozami 1980; Chambers, Murphy & McEligot 1982; Van Maanen 1980; Johansson & Alfredsson 1982; Willmarth & Sharma 1983) the same technique was adopted here.

2. Equipment

A closed-return wind tunnel was used in this experiment. The flow field was established by a 42 in diameter nine-blade axial fan powered by a 25 horsepower variable-speed d.c. motor. Downstream of the fan, the flow expanded through a $5\frac{1}{2}°$ diffuser until the cross-sectional flow area was $2{\cdot}5 \times 2{\cdot}5$ m. After two 90° turns, the flow passed through a 10 cm long honeycomb having 0·48 cm cells. The screen section consisted of 4 individual damping screens; the first 3 were 20×20 mesh screens having an open area of 53 % followed by a 24×24 mesh screen having an open area of 72 %. The settling chamber downstream of the screens was 1·8 m long before the flow entered a two-dimensional contraction into the test section. The test section had a cross-sectional area of 60×90 cm and was 6·0 m long. After exiting from the test section the flow encountered two 90° turns before the fan. All of the 90° turns within the tunnel were equipped with turning vanes. The turbulence level within the test section was less than 0·05 % at all free-stream velocities. The maximum velocity in the test section was 20 m/s in its present configuration.

A 90×600 cm flat plate was installed in the test section. The first 360 cm was a 0·6 cm thick aluminium plate reinforced on the backside so that it was flat within 0·01 mm. The remaining 240 cm of the flat plate was Plexiglas. The junction between the aluminium and Plexiglas plates was aerodynamically smooth such that the surface discontinuities were less than 0·01 mm everywhere. The leading edge of the aluminium plate was round. At the trailing edge of the Plexiglas plate, a flap was installed to control the stagnation point at the leading edge.

In addition to studying the naturally occurring turbulence within the boundary layer, two different boundary-layer trips were used. The first type of trip consisted of two staggered rows of inverted rivets spaced 2 cm apart in the spanwise direction. The distance between the rows was 1 cm. The rivets were located 45 cm downstream from the leading edge, and when glued to the plate extended 0·8 cm above the plate.

The second trip consisted of sheets of No. 24 carborundum metal cloth glued over the initial 56 cm of the flat plate and covered the entire span of the plate.

Data for the present research were taken using both individual hot-wire probes and a hot-wire rake. In both cases, the hot-wire sensors were attached to jewellers' broaches extending upstream from the probe support approximately 1·5 cm. The jewellers broaches were tapered to a diameter of 0·05 mm at the tip. In the individual probes, the broaches were spaced at various distances so that a variety of hot wires having different lengths could be used. The sensing elements of the hot-wire probes were soft-soldered directly onto the broaches. Platinum–10 % rhodium wires having diameters ranging from 1.2 to 5.0 μm were used.

The hot-wire anemometers used in this experiment were the same as those described by Blackwelder & Kaplan (1976). Overheat ratios of nominally 33 % were used throughout this investigation. By using higher and lower values, the effect of the overheat ratio was found to be nil. Depending upon the diameter of the hot-wire sensor, the frequency response of the anemometers varied from 5 to 12 kHz. The output signals from the anemometers entered a bucking amplifier, which subtracted a fixed voltage and amplified the remaining signal by a factor of 10. These signals were connected to analog-to-digital converters, which were controlled by a PDP 11/55 computer and were capable of digitizing data at the rate of 350000 samples/s. However, to acquire digital data continuously in time without inter-record gaps, the acquisition speed was limited by the transfer rate to the disk pack. By using double buffering, a maximum aggregate digitizing rate of 240 kwords/s was possible, giving data which were continuous in time from one block to the next. The digitized velocities were stored on an 80 Mbyte Winchester disk for further processing. During calibration, the hot-wire sensors were placed in the free stream near a Pitot–static tube. The resulting pressure difference at each velocity was measured by an MKS Baratron pressure transducer. The pressure signal was also digitized during calibration, and Bernoulli's equation used to obtain the free-stream velocity. The acquired data set for each run was typically linearized and written onto a magnetic tape for permanent storage. All of the remaining digital processing was accomplished on the PDP 11/55 computer using FORTRAN programs. A 4010 Tektronix terminal was used to communicate with the computer as well as to display the graphical output of the data.

3. Experimental procedure

3.1. *Calibration of the hot wires*

The hot wires were always calibrated in the free stream of the wind tunnel just prior to recording the data. First, the Baratron pressure transducer was calibrated by digitizing and recording the output voltage corresponding to four known pressure settings. A linear least-squares fit of this data was consequently used to obtain the pressure readings from the Pitot tube at different free-stream velocities. The frequency response of the hot wires was set using the square-wave technique at the maximum velocity to be encountered in the subsequent data run. The calibration of the hot wires proceeded in a similar manner to that of the Baratron. Since the data were typically recorded at $y^+ = 15$ where $0{\cdot}4 < \bar{U}/U_\infty < 0{\cdot}6$, the wind tunnel was run at approximately six different velocities ranging from 5 % to 100 % of the free-stream velocity. At each calibration velocity, approximately five seconds of data were recorded and averaged for each hot-wire channel and the pressure transducer.

The velocity was calculated using the recorded pressure signal and Bernoulli's equations. A polynomial of typically third order was found sufficient to form a least-squares fit of the anemometer's voltage versus the velocity. The same program with a variable array was used to calibrate the hot-wire rakes. This usually required no more real time than to calibrate a single probe; i.e. nominally 5 min. Immediately after calibration, the sensors were positioned in the boundary layer and the data recorded. Upon completion, the probes were returned to the free stream and the calibration checked. If any of the sensors had drifted more than 1–2 %, the data were rejected; the calibration process was repeated and new data recorded.

3.2. *Velocity measurements*

The velocity profiles were obtained early in the program to verify that a standard boundary layer was obtained. The relative distance from the wall was entered into the computer and the velocity was recorded from which the mean and r.m.s. were immediately calculated. These data were plotted on the Tektronix terminal and the probe moved to the next location. By using this technique near the wall, the linear region of the mean velocity profile could be identified and extrapolated to determine the absolute distance from the wall. A telescope was used to verify this distance by viewing the sensor and its mirror image. This method was also used to determine if the wire was parallel to the wall.

From the mean-velocity profiles (see figure 2) it is ascertained that the mean velocity at $y^+ = 15$ was $12u_\tau$.† This criterion was used for locating $y^+ = 15$ when recording the bursting-frequency data, giving a maximum error of $\Delta y^+ = \pm 2$ at all Reynolds numbers used in the investigation. This method was less time-consuming than determining the absolute distance from the wall. For calculating the bursting period, the temporal record length was taken to be $1000\delta/U_\infty$: i.e. the passage time of several hundred large eddies in the outer flow. The data were always digitized and recorded continuously in time. The digitizing interval was typically equal to ν/u_τ^2.

Immediately after linearizing the data, the mean and r.m.s. values at $y^+ = 15$ were calculated for all channels and checked against standard values. At all Reynolds numbers the r.m.s. streamwise velocity was approximately $3u_\tau$. For the hot-wire sensors having a long length, i.e. $l^+ > 20$, the r.m.s. velocity was slightly less than $3u_\tau$. This result was expected because the long sensor has poor spatial resolution and averages over the fluctuations having a spanwise scale less than the wire length. This effect seemed independent of the length-to-diameter ratio.

More surprisingly, low r.m.s. values were also obtained for short sensors having $l/d < 200$. Fluctuation values as low as $2{\cdot}0u_\tau$ were observed for $l/d = 50$, and $2{\cdot}5u_\tau$ for sensors having $l/d = 100$. This result seemed independent of the sensor length when scaled with the viscous wall parameters l^+ and could not be adequately explained. One possibility is that, since the sensors were soldered directly onto the prongs, the closely spaced prongs may have caused some probe interference. Another explanation is that the strongly non-uniform temperature distribution along the

† The friction velocity u_τ was determined by the velocity gradient at the wall, which yielded a larger scatter in the data in the logarithmic region seen in figure 2. The characteristic velocity u^* obtained from the slope of the logarithmic region was typically 15 % greater than u_τ. Using u^* to normalize the data in figure 2 reduced the scatter in the logarithmic region but increased it in the wall region. Since the scatter at $y^+ = 15$ was smaller using the friction velocity u_τ, it was used to normalize all the data reported here. For completeness, the values of both u_τ and u^* are included in table 1. It should be noted that, at $y^+ = 15$, $\overline{U}/u^*$ was typically 10·5 in agreement with previous results.

sensor promotes and/or acts in collusion with a time-dependent heat transfer into the supporting prongs, thus causing a temporal averaging of the heat transfer. This problem is being studied further. Since the r.m.s. values from sensors having $l/d < 200$ could not be adequately explained, those results were not used in the following.

3.3. *Detection criterion*

Several different detection techniques could have been employed in this work to determine the bursting interval. However, the purpose was not to compare different methods but rather to choose one detection technique that could be utilized over the entire Reynolds-number range. The variable-interval time-averaging method introduced by Blackwelder & Kaplan (1972) has been used under the most diversified conditions, as discussed earlier. Since it could easily be employed over the entire Reynolds-number range with the same parameters, it was adopted.

The variable-interval time average of a fluctuating quantity $Q(x_i, t)$ is defined by

$$\hat{Q}(x_i, t, \tau) = \frac{1}{\tau} \int_{t-\frac{1}{2}\tau}^{t+\frac{1}{2}\tau} Q(x_i, s)\, ds, \tag{1}$$

where τ is the averaging time. This average $\hat{Q}(x_i, t, \tau)$ is effectively a low-pass filter having zero phase shift applied to the original function. As the averaging time τ becomes large compared with the timescales of $Q(x_i, t)$, the conventional time average $\bar{Q}(x_i)$ results; i.e.

$$\bar{Q}(x_i) = \lim_{\tau \to \infty} \hat{Q}(x_i, t, \tau). \tag{2}$$

A localized measure of the turbulent energy associated with the fluctuations is obtained by applying the VITA technique to the square of the fluctuations. For the streamwise velocity component, the fluctuating velocity is

$$u(x_i, t) = U(x_i, t) - \bar{U}(x_i), \tag{3}$$

and the VITA measure of its energy is the variance given by

$$\widehat{\mathrm{var}}\,(x_i, t, \tau) = \widehat{u^2}(x_i, t, \tau) - [\hat{u}(x_i, t, \tau)]^2.$$

Since $\hat{u}(x_i, t, \tau) \to 0$ as $\tau \to \infty$, the variance yields the total energy in the limit

$$\lim_{\tau \to \infty} \widehat{\mathrm{var}}\,(x_i, t, \tau) = u^2_{\mathrm{rms}}(x_i).$$

As shown by Blackwelder & Kaplan (1976), $\widehat{\mathrm{var}}\,(x_i, t, \tau)$ is a positive-definite quantity having a large positive skewness. The large excursions are associated with accelerations and/or decelerations of the streamwise velocity signal from the local mean. Chen & Blackwelder (1978) reported that the more important aspects of the bursting phenomenon were due primarily to the accelerations, and thus did not study the decelerations. That criterion was also adopted, so the detection function $D(t)$ used in this investigation is defined as

$$D(t) = \begin{cases} 1 & \text{if } \widehat{\mathrm{var}} > k u^2_{\mathrm{rms}} \text{ and } \dfrac{du(t)}{dt} > 0, \\ 0 & \text{otherwise,} \end{cases}$$

where k is the threshold value.

The bursting frequency f is obtained from this method by counting the number of times that $D(t)$ changes from zero to unity per unit time interval. In practice this frequency depends upon the two detection parameters τ and k, as well as the spatial

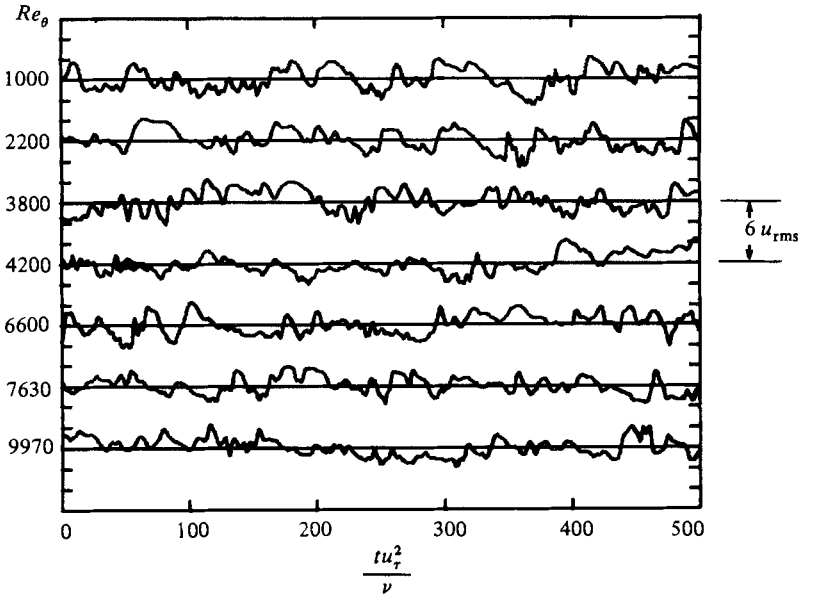

FIGURE 1. Comparison of the instantaneous streamwise velocity signals at $y^+ = 15$ and various Reynolds numbers. The data are normalized by their r.m.s value.

location x_i of the sensing probe. Homogeneity implies that the mean frequency cannot be a function of the streamwise and spanwise positions x and z. The bursting frequency is only a weak function of the distance from the wall, as seen later. The nominal location used for measuring the bursting frequency was chosen as $y^+ = 15$ because the turbulent production is maximized there, and Blackwelder & Kaplan (1976) found the largest educed signatures from the eddy structure at that location.

By examining the definition of the bursting frequency, it is apparent that no unique value of the threshold can be obtained by searching for a region were f is relatively independent of k. Chen & Blackwelder (1978) have shown that, whenever a simple threshold level is applied to a function having a continuous probability distribution, the frequency of occurrence will vary monotonically with the threshold parameter. Thus no region can be found where the results will be independent of the threshold parameter, i.e. constant over a range of k. Consequently no attempt was made to determine the variation of f as the threshold changed and k was set equal to unity for all of the following results. It should be noted that, in the VITA and other detection techniques, almost any value of f could have been obtained by choosing other values of the threshold. Consequently, no great significance can be placed on the absolute values of f recorded. However, since k was held constant for all of the data, the relative variation of the frequency reported here cannot be attributed to the threshold value.

A comparison of the data at different values of the Reynolds number was deemed necessary before determining the averaging interval τ. Figure 1 shows a sample of the data at $y^+ = 15$ for seven values of the Reynolds number studied. Note that the time records in the figure are scaled with the wall variables ν and u_τ, and no significant differences are observed over the Reynolds-number range. However, when scaled with U_∞ and the boundary-layer thickness δ, considerable differences in the frequency content of the signals were observed because of the compression imposed by the time-scale. Comparisons of spectra also revealed that the only timescale appropriate for this data was ν/u_τ^2. Consequently the averaging time τ was chosen so that $\tau u_\tau^2/\nu = 10$

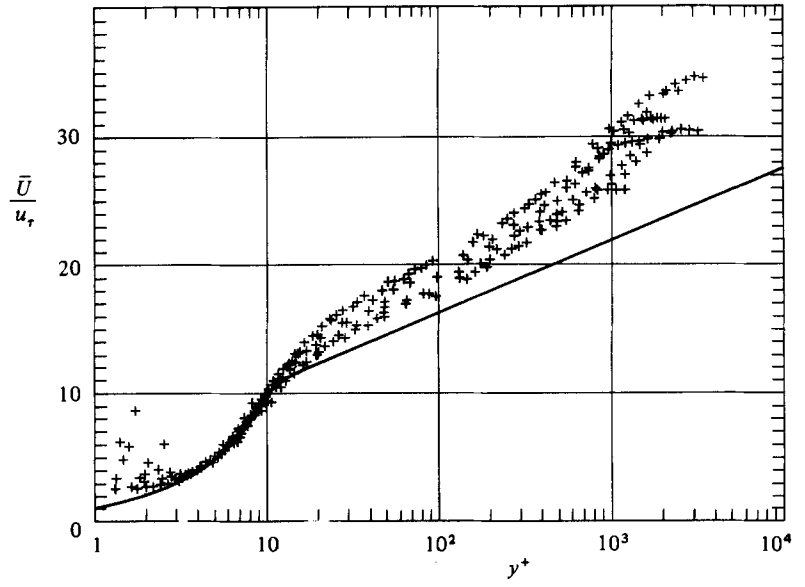

FIGURE 2. Mean-velocity profiles over the Reynolds-number range $10^3 < Re_\theta < 10^4$. The solid line is given by $U/u_\tau = y^+$ for $y^+ < 11$ and by $(1/0.41)\ln y + 5.0$ for $y^+ > 11$. The friction velocity was obtained from the linear region near the wall, thus causing a better collapse of the data there.

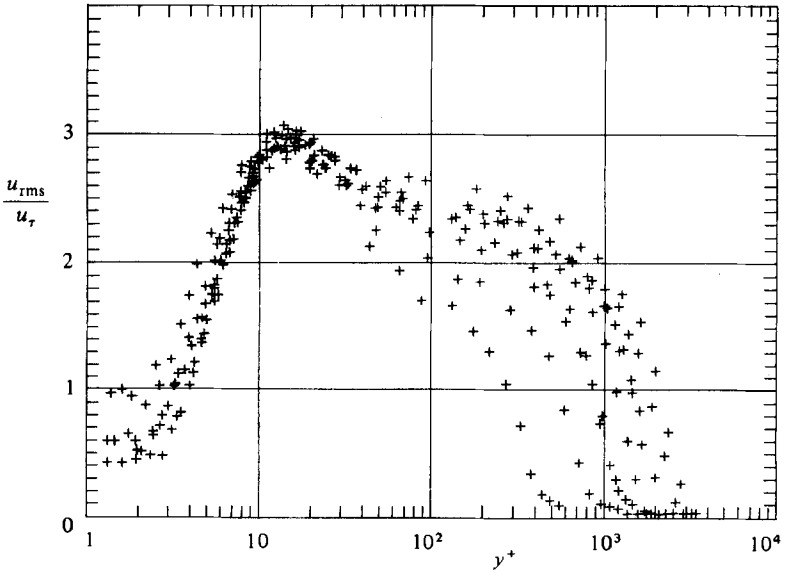

FIGURE 3. The fluctuating streamwise velocity profiles obtained for the same conditions as in figure 2.

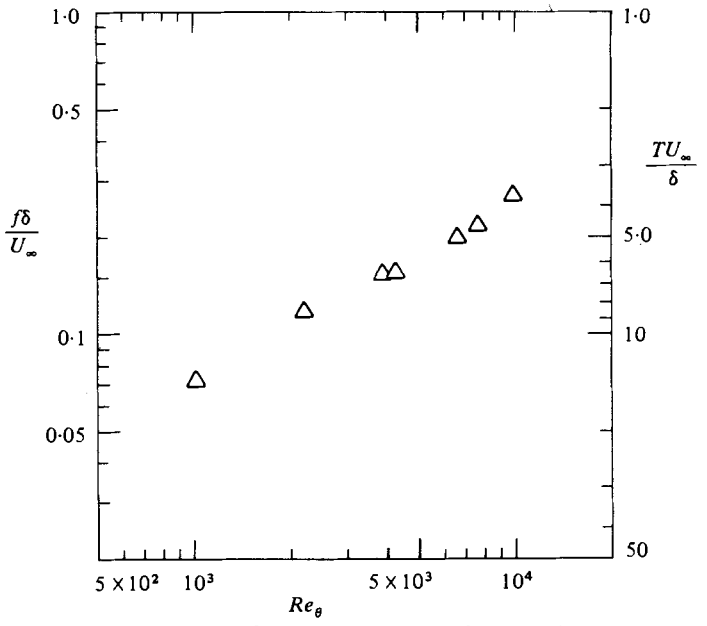

FIGURE 4. The mean bursting frequency scaled with outer flow variables obtained with a 2·5 μm diameter hot-wire sensor having a length of 0·5 mm.

for all of the data analysed. Although the absolute value of the bursting frequency is dependent upon the non-dimensional averaging interval τ^+, the observed trends with Reynolds number cannot be ascribed to this variable, since it was held constant.

4. Results

4.1. *Mean statistics*

The mean and r.m.s. velocity profiles are shown in figures 2 and 3 respectively. These data were taken using a 1 mm long, 2·5 μm diameter sensor having $l/d = 400$. The viscous lengthscale of the wire varied between $l^+ = 9$ and 40 over the Reynolds-number range 10^3–10^4. The data were recorded at three different streamwise locations of $x = 2$, 3·5 and 5 m from the leading edge. The free-stream velocity was varied to obtain similar Reynolds numbers at different locations whenever possible. Data were also recorded at the same Reynolds number with natural transition and the two different boundary-layer trips. None of these differences produced any anomalous results. In addition, the law of the wake component was checked separately with similar agreement.

The friction velocity obtained from the velocity gradient at the wall u_τ was used to normalize the data. Since u_τ was typically 15 % less than the characteristic velocity obtained from the slope of the logarithmic region, the data lie above the standard curve and have a larger slope. No corrections have been applied to compensate for the conduction to the wall, which explains the enhanced velocity values at $y^+ < 3$.

4.2. *Bursting frequency*

The bursting frequency recorded over the Reynolds-number range 10^3–10^4 is shown in figure 4. Since Rao *et al.* (1971) have suggested that the frequency should be constant when normalized with the outer variables, that scaling is used in the figure.†

† The mean bursting frequency is the primary variable of interest. Its inverse, the mean time between bursts, is recorded on the right-hand side of this and subsequent figures.

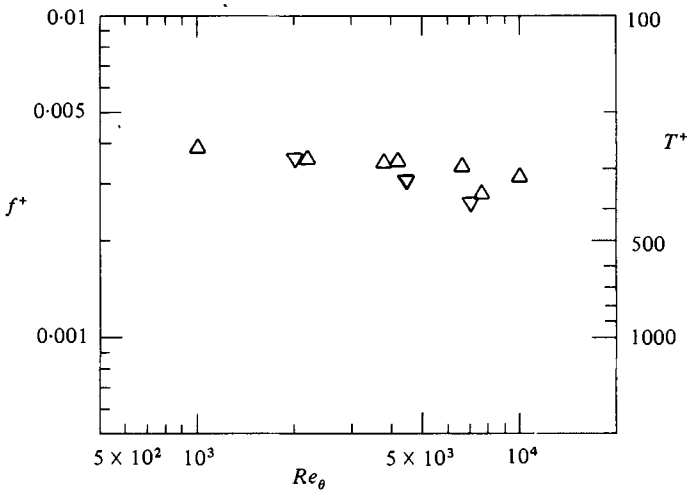

FIGURE 5. The mean bursting frequency scaled with the wall variables ν and u_τ. In addition to the data from figure 4 three other points from an untripped boundary layer are added.

These original data were all recorded with a 2·5 μm diameter, 0·5 mm long hot wire, which had a viscous lengthscale in the range $4{\cdot}5 < l^+ < 20$. As can be seen, the data are not constant verus Re_θ but increased like $Re_\theta^{0.6}$. Willmarth & Sharma (1983) have used the same technique with minor modifications at $Re_\theta = 6000$ and 13000, and observed the same Reynolds-number dependence. Their values were slightly lower than those in figure 4 owing to slight differences in the sensors and the detection criterion. Chambers *et al.* (1982) used the VITA detection technique in a channel flow and also found the same Reynolds-number dependence.

When the same data are plotted using the viscous wall parameter to normalize the frequency, figure 5 results. It is readily evident that f^+ is approximately constant over the Reynolds-number range and has a nominal value of 0·0035. This yields an average interval between bursts of typically $300\nu/u_\tau^2$ independent of the Reynolds number. The previously mentioned data of Willmarth & Sharma and Chambers *et al.* also yield a constant value for all Reynolds numbers when scaled with the wall variables. The bursting frequency using the same technique and parameters obtained by Blackwelder & Eckelmann (1978) in a channel flow yields a value of $f^+ = 0.0041$ at $Re_\theta = 400$ in agreement with figure 5. Also included in the figure are data points obtained in a boundary layer with natural transition. These, and other data taken with the sandpaper trip, agree well with data obtained downstream of the rivet trip, indicating that f^+ is independent of the boundary-layer origin.

When the characteristic velocity, u^* instead of u_τ was used to normalize the bursting frequency, the value of f^+ was shifted by approximately 30 % and a slightly larger scatter was seen in the data. However, the same conclusion was obtained; namely f^+ was constant over the Reynolds-number range.

The overwhelming conclusion from this figure, and the primary conclusion of this investigation, is that the bursting frequency scales with the wall parameters and is independent of the Reynolds number. Since this result is contrary to that of Rao *et al.* (1971), an explanation of this discrepancy was attempted as described below.

4.3. *Effect of digitizing frequency*

There is no immediate reason why the digitizing frequency should affect the above results. Nevertheless, one set of data at $Re_\theta = 2200$ was recorded at a significantly

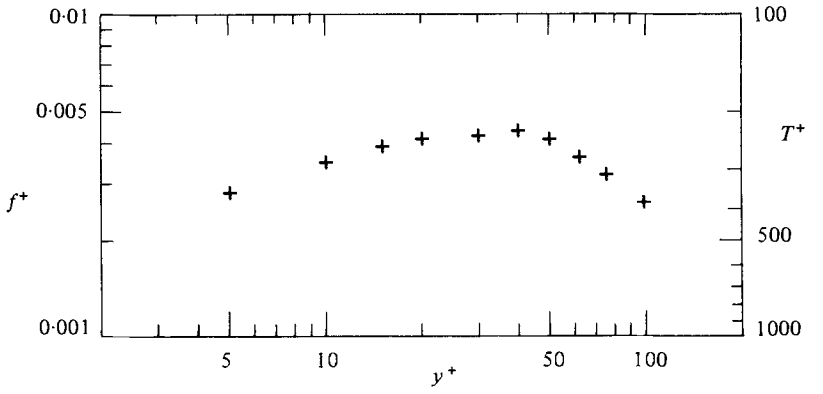

FIGURE 6. The variation of the bursting frequency across the wall region.

faster rate, i.e. the interval between samples was $\Delta t = 0{\cdot}28\nu/u_\tau^2$. From this basic data set, other sets could be derived having an effective digitizing rate of $n\Delta t$, where $n = 1, 2, \ldots$. From these derived data sets, the detection scheme was applied such that $\tau^+ = 10$ always; i.e. the non-dimensional averaging interval had the same length but contained a differing number of data points in each average. There was no effect upon the calculated bursting frequency as long as the digitizing interval was significantly less than the averaging interval, i.e. $\Delta t \ll \tau$.

4.4. *Effect of detection location*

Rao *et al.* (1971), Chen & Blackwelder (1978) and others have shown that the burst count per unit time using the same detection technique is fairly constant across the boundary layer. The results of the present study are shown in figure 6 for $5 \leqslant y^+ \leqslant 100$ and $Re_\theta = 2500$. Although a slight variation is observed, the conclusion is that the frequency is approximately a constant throughout the wall region.

4.5. *Frequency dependence upon sensor length*

The bursting phenomenon is associated with streamwise vortices and streaks of low-speed fluid in the wall having small physical scales. Lee, Eckelmann & Hanratty (1974) and Oldaker & Tiederman (1977) have shown that the median streak spacing in the spanwise direction at low Reynolds numbers is approximately $80\nu/u_\tau$ and the mean is $100\nu/u_\tau$. In addition, Corino & Brodkey (1969) observed strong velocity gradients over a spanwise distance of $20\nu/u_\tau$ and Willmarth & Bogar (1977) found evidence near the wall of scales less than the Kolmogorov length. So it is expected that the sensor length in the spanwise direction will be important in detecting the bursts, especially if the length exceeds approximately $20\nu/u_\tau$. Initially data were recorded with 2·5 μm diameter hot wires having length/diameter ratios of 50, 100, 200, 400 and 800. The wires having $l/d = 50$ and 100 always recorded u' values that were too small as discussed earlier and thus they were not used. (The mean bursting frequencies recorded from these sensors were typically low with considerable scatter.) Other sensors having different diameters and lengths were also used. The bursting frequencies from the sensors tested are shown in figure 7, and the relevant parameters are given in table 1. At the low Reynolds numbers there is general agreement, but considerable scatter is evident at the higher values, suggesting that almost any value of f^+ can be obtained depending upon the sensor size.

Upon closer examination, a trend can be noticed for each of the longer sensors; namely the frequency decreases as the Reynolds number increases. The hot-wire

Re_θ	x (cm)	U_∞ (cm/s)	$\frac{u_\tau}{U_\infty}$	$\frac{u^*}{U_\infty}$	Diameter (μm)	l/d	l^+	$\frac{f\delta}{U_\infty}$	f^+	Trip†	Plotting symbol
1000	200	310	0·043	0·047	2·5	200	4·5	0·072	0·0039	R	△
2200	200	740	0·039	0·042	2·5	200	9·8	0·119	0·0036	R	△
3800	350	880	0·034	0·039	2·5	200	10·1	0·154	0·0035	R	△
4200	200	1500	0·032	0·038	2·5	200	16·3	0·153	0·0036	R	△
6600	350	1720	0·030	0·036	2·5	200	17·5	0·201	0·0034	R	△
7630	500	1510	0·033	0·036	2·5	200	16·9	0·218	0·0026	R	△
9970	500	1930	0·029	0·036	2·5	200	19·0	0·272	0·0032	R	△
1000	200	310	0·043	0·047	1·3	200	2·3	0·071	0·0038	R	▽
2070	500	500	0·039	0·043	1·3	200	3·3	0·115	0·0036	N	▽
2200	200	752	0·039	0·042	1·3	200	5·0	0·130	0·0039	R	▽
4500	500	1075	0·035	0·038	1·3	200	6·4	0·166	0·0030	N	▽
6500	500	1220	0·033	0·037	1·3	200	6·8	0·222	0·0031	R	▽
6950	500	1955	0·033	0·036	1·3	200	10·9	0·200	0·0026	N	▽
10000	500	1960	0·029	0·036	1·3	200	9·6	0·286	0·0034	R	▽
2000	500	483	0·039	0·043	2·5	400	12·8	0·090	0·0030	N	◇
4100	500	1006	0·035	0·038	2·5	400	23·8	0·136	0·0027	N	◇
5300	500	1350	0·034	0·037	2·5	400	31·1	0·137	0·0022	N	◇
5700	500	1500	0·033	0·037	2·5	400	33·5	0·106	0·0017	N	◇
7000	500	1980	0·033	0·036	2·5	400	44·3	0·087	0·0011	N	◇
1000	200	311	0·043	0·047	2·5	800	18·1	0·057	0·0031	R	□
2100	500	497	0·035	0·038	2·5	800	23·6	0·097	0·0032	N	□
2400	500	501	0·039	0·042	2·5	800	26·5	0·092	0·0025	R	□
4200	500	1000	0·035	0·038	2·5	800	47·4	0·080	0·0016	N	□
6500	500	1220	0·033	0·037	2·5	800	54·5	0·091	0·0013	R	□
6810	500	1920	0·033	0·036	2·5	800	85·8	0·057	0·0008	N	□
10000	500	1970	0·029	0·036	2·5	800	77·4	0·069	0·0008	R	□
6500	500	1220	0·033	0·037	1·3	1600	54·5	0·103	0·0015	R	○
10000	500	1940	0·029	0·036	1·3	1600	76·2	0·078	0·0009	R	○

† R = rivet trip, N = natural transition.

TABLE 1

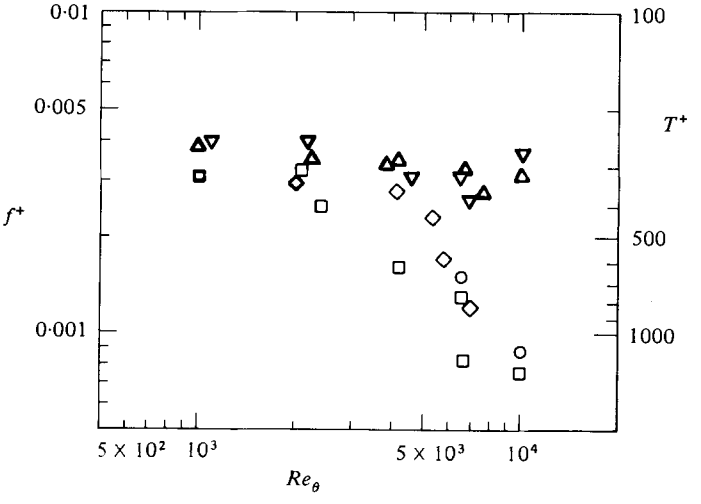

FIGURE 7. The mean bursting frequency scaled with wall variables obtained from hot-wire sensors having different diameters and lengths. The symbols are given in table 1. The sensors with $l^+ < 20$ are denoted by the symbols with the bold outlines.

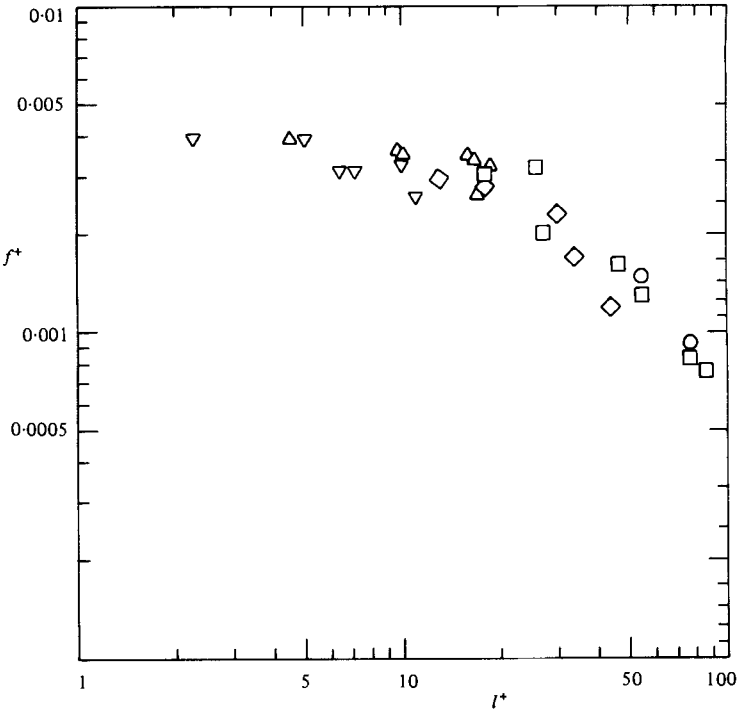

FIGURE 8. The mean bursting frequency at different Reynolds numbers versus the length of the sensor. Symbols are given in table 1.

signal is proportional to a spanwise average over its length; thus it is expected that some signal degradation will occur whenever the sensor's length exceeds the spanwise scale of the energetic eddies. Indeed the r.m.s. values recorded by the longer wires was typically lower than those having shorter lengths. Lee *et al.* (1974) and Oldaker & Tiederman (1977) have shown that there is a continuous distribution of spanwise scales of the low-speed streaks ranging from 20 to $200\nu/u_\tau$. Consequently, sensors having lengths greater than $20\nu/u_\tau$ would be larger than some of the streaks. Blackwelder (1979) has suggested that the detection scheme triggers on the abrupt ending of a low-speed streak; consequently some of the bursts would be missed by the longer sensor, causing a reduced frequency. Since the characteristic lengthscale in the wall region ν/u_τ typically decreases as the Reynolds number increases, this could explain the trend seen in the figure.

On the other hand, the data obtained from sufficiently small sensors showed that f^+ was approximately a constant over the Reynolds-number range tested. This suggests that the only relevant independent variable in figure 7 is the wire length, indicating that a better collapse of the data would be obtained by graphing f^+ versus the sensor length scaled on wall variables. The same data are replotted in figure 8, showing that they do follow a single curve. That is, given the sensor length, a unique value of the bursting frequency is obtained.

Two interesting observations can readily be made from this figure. First, f^+ is essentially constant for all sensors having a lengthscale less than $20\nu/u_\tau$. This suggests that the spanwise extent of the most-energetic eddies must be greater than $20\nu/u_\tau$. If not, the frequency should continue to change for the shorter hot wires. Secondly, if the sensors are indeed averaging over the bursting structure as a simple first-order

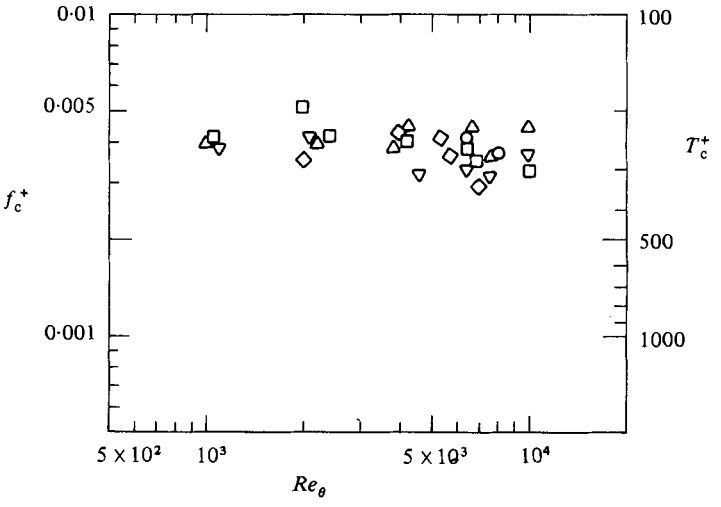

FIGURE 9. The mean bursting frequencies corrected for the spatial averaging of the sensor.

spatial filter, the slope of the roll-off should be 6 dB/octave. Within the scatter of the data, this appears to be true. By analogy with the first-order temporal filter, a correction for the wire length can be obtained. Namely the corrected frequency f_c is given by

$$f_c^+ = f^+[1 + (\tfrac{1}{20}l^+)^2]^{\frac{1}{2}},$$

where f^+ is the recorded frequency and $l^+ = 20$ is the 3 dB point of the spatial filter. When f_c^+ is plotted versus l^+ the data are approximately constant over the entire range. Since this correction removes the effect of the sensor size, the corrected data can be replotted versus the Reynolds number as in figure 9. Under the above conditions, the data indicate that the bursting frequency scaled with the wall parameters is indeed a constant and independent of the Reynolds number.

5. Discussion

The results of § 4 show that the mean bursting frequency scales with the inner wall variables ν and u_τ. However, they do not explain how Rao *et al.* (1971) concluded that the outer flow variables δ and U_∞ were the appropriate scaling parameters. A review of their work including their 1969 report suggests that they may have encountered significant spatial averaging with their sensors. Their test section was only 8 ft long, and a maximum velocity of 100 ft/s was used; consequently their viscous lengthscales were typically smaller than those of this investigation. Lacking sufficient information to apply a correction of the type in figure 9 to their data, a similar set of data was taken to simulate their results. A 2·5 μm diameter hot-wire 2 mm long was used over the entire Reynolds number range. These data are given in table 1 and have been used in the previous figures. The same data are shown in figure 10 scaled with the outer flow variables. The scatter in the data is no worse than the scatter in the data of Rao *et al.* (1971), and, when viewed by itself, the figure strongly suggests that the outer variables may indeed be the appropriate scaling device. The wire length varied between 18 and $85\nu/u_\tau$ over the Reynolds-number range shown in figure 10, compared with 14 and $54\nu/u_\tau$ over the Reynolds-number range of 600–9000 in their experiments. For these wire lengths figure 8 shows that

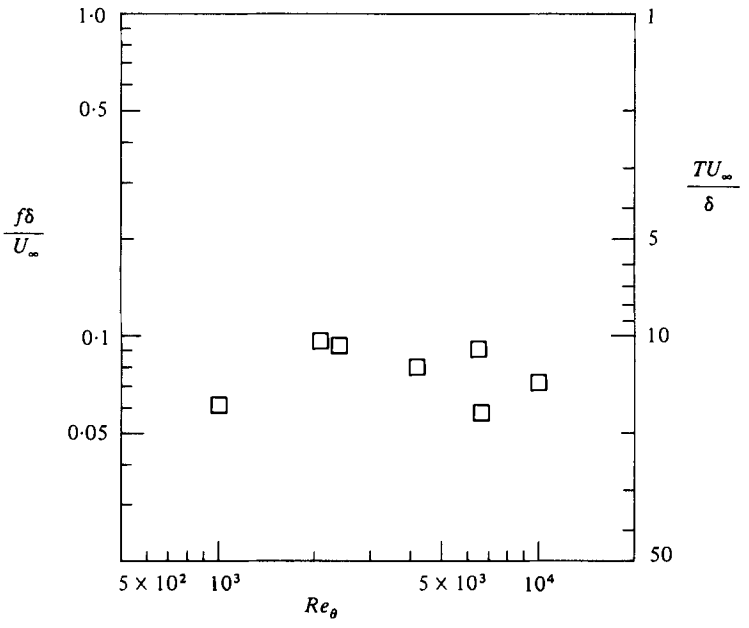

FIGURE 10. Uncorrected mean bursting frequency scaled on outer flow variables obtained with a 2 mm long hot wire. The length of the wire varied from 18 to $85\nu/u_\tau$ over the above Reynolds-number range.

f^+ decreases like $(l^+)^{-1}$. Rescaling this frequency with the outer variables shows that it is approximately constant with Reynolds number. Thus it appears that the results of Rao *et al.* (1971) were due to the averaging effects of their sensor.

It should be recalled that the detection technique of Rao *et al.* triggered on oscillations of a turbulent signal after it was passed through a narrow band-pass filter. Ueda & Hinze (1975) used a similar detection technique on signals from a hot-wire sensor having $l/d = 100$ at two Reynolds numbers differing by a factor of three. They found that the detection rate was constant when scaled with outer variables in spite of the fact that the lengthscales and spectra of the u-signal and its first two derivatives scaled with the viscous parameters. They emphasize that their results are related to the fine structure of turbulence; thus the narrow-band filtering may be detecting a different aspect of the turbulent structure. For example, the bursts detected by the VITA technique are correlated with large Reynolds stress, but such a relation has never been studied using the detection technique of Rao *et al.*

More recently, Alfredsson & Johansson (1982) have proposed that the geometrical mean of the inner and outer timescales is the appropriate scale for the bursts detected by the VITA technique in a channel flow. This new idea was tested on the data reported here. However, the non-dimensional frequencies obtained using their methodology still scaled better with the inner variables rather than with the mixed timescales.

6. Conclusion

The primary conclusion of this research is that the mean bursting frequency scales with the inner viscous variables u_τ and ν and not with the outer variables δ and U_∞. The idea that the bursting frequency should scale with the wall variables is not new. Indeed if this phenomenon is only a wall-layer process, there is no other alternative

but the wall parameters. Black (1966) modelled the bursting process using a ν/u_τ^2 timescale, and Kline *et al.* (1967) and Corino & Brodkey (1969) both showed that their data scaled with ν and u_τ, although their Reynolds-number ranges were quite limited. Other visualization and probe data have supported this scaling also, although always over a limited Reynolds-number range; e.g. Donohue, Tiederman & Reischman (1972) in channels and Achia & Thompson (1977) in pipe flows.

When scaled with the wall variables, a very weak dependence on Reynolds number may be inferred from the data. For example, f^+ appears to decrease sightly in figures 5 and 9 as the Reynolds number increases, but the scatter precludes any definite conclusions.

Blackwelder & Eckelmann (1978) used the same detection process and parameters in an oil channel as used in this investigation. Their data yields $f^+ = 0.0041$ at $y^+ = 15$ and $Re_\theta =$ using a 1 mm long ($l^+ = 1.5$) hot-film probe. This agrees with and extends the range of data in figures 5–9, but these data were not included explicitly because the flow field was a turbulent channel and not a boundary layer. However, since the mean bursting frequency is independent of the outer flow variables, there is now no reason to exclude them. The similarity between the wall structure in these two flow fields is further supported by the fact that the educed structure of Blackwelder & Eckelmann agrees with that of Blackwelder & Kaplan (1976) when scaled with the wall variables. Thus a strong argument can be made that the bursting phenomenon is universal in boundary layers, pipes and channels.

This investigation also concludes that the sensor size is a more important parameter than was previously believed. Willmarth & Sharma (1983) have shown that extremely small sensors measured more energy in the smaller scales of the spectrum. The present results suggest that, whenever the signals are subjected to higher-order analysis such as that involved in the detection algorithm, the spatial resolution problem may become more acute.

The authors gratefully acknowledge the financial support for this research provided by the Army Research Office, Durham, under Grant DAAG29-79-C-0137, and by the Air Force Office of Scientific Research through Grant F49620-78-C-0060. We also thank Professors John Laufer and Richard Kaplan for their helpful discussions during the course of this investigation and Professor Roddam Narasimha for reviewing the manuscript.

REFERENCES

ACHIA, B. U. & THOMPSON, D. W. 1977 *J. Fluid Mech.* **81**, 439.

ALFREDSSON, P. H. & JOHANSSON, A. V. 1982 Timescales for turbulent channel flow. *Royal Inst. Tech., Stockholm, Rep.* TRITA-MEK-82-11.

BAKEWELL, H. P. & LUMLEY, J. L. 1967 *Phys. Fluids* **10**, 1880.

BLACK, T. J. 1966 In *Proc. Heat Transfer and Fluid Mechanics Institute*, p. 366. Stanford University Press.

BLACKWELDER, R. F. 1979 In *Coherent Structures of Turbulent Boundary Layers* (ed. C. R. Smith & D. E. Abbott), p. 211. Lehigh University.

BLACKWELDER, R. F. & ECKELMANN, H. 1978 In *Structure and Mechanism of Turbulence* (ed. H. Fiedler). Lecture Notes in Physics, p. 190. Springer.

BLACKWELDER, R. F. & KAPLAN, R. E. 1972 *Intermittent Structures in Turbulent Boundary Layers, NATO–AGARD* CP 93. London: Technical Editing and Reproduction.

BLACKWELDER, R. F. & KAPLAN, R. E. 1976 *J. Fluid Mech.* **76**, 89.

BROWN, G. L. & THOMAS, A. S. W. 1977 *Phys. Fluids Suppl.* **20**, S243.

CHAMBERS, F. W., MURPHY, H. D. & MCELIGOT, D. M. 1983 *J. Fluid Mech.* **127**, 403.

CHEN, C. H. P. & BLACKWELDER, R. F. 1978 *J. Fluid Mech.* **89**, 1.

COLES, D. 1979 In *Coherent Structures of Turbulent Boundary Layers* (ed. C. R. Smith & D. E. Abbott), p. 462. Lehigh University.

CORINO, E. R. & BRODKEY, R. S. 1969 *J. Fluid Mech.* **37**, 1.

DONOHUE, G. L., TIEDERMAN, W. G. & REISCHMAN, M. M. 1972 *J. Fluid Mech.* **56**, 559.

FALCO, R. 1980 *Production of Turbulence Near a Wall, AIAA*-80-1356.

JOHANSSON, A. V. & ALFREDSSON, P. H. 1982 *J. Fluid Mech.* **122**, 295.

KIM, H. T., KLINE, S. J. & REYNOLDS, W. D. 1971 *J. Fluid Mech.* **50**, 733.

KLINE, S. J., REYNOLDS, W. C., SCHRAUB, J. A. & RUNSTADLER, P. W. 1967 *J. Fluid Mech.* **30**, 741.

LAUFER, J. & BADRI NARAYANAN, M. A. 1971 *Phys. Fluids* **14**, 182.

LEE, M. K., ECKELMANN, L. D. & HANRATTY, T. J. 1974 *J. Fluid Mech.* **66**, 17.

OLDAKER, D. & TIEDERMAN, W. G. 1977 *Phys. Fluids Suppl.* **20**, S133.

RAO, K., NARASIMHA, R. & BADRI NARAYANAN, M. A. 1969 *Ind. Inst. Sci. Rep.* 69FM8.

RAO, K., NARASIMHA, R. & BADRI NARAYANAN, M. A. 1971 *J. Fluid Mech.* **48**, 339.

SCHRAUB, F. A. & KLINE, S. J. 1965 *Stanford University Rep.* MD-12.

SMITH, C. R. & ABBOTT, D. E. (eds) 1979 *Coherent Structures of Turbulent Boundary Layers.* Lehigh University.

UEDA, H. & HINZE, J. O. 1975 *J. Fluid Mech.* **67**, 125.

VAN MAANEN, H. R. E. 1980 In *Turbulent Boundary Layers – Experiments, Theory and Modelling, AGARD* CP 271, p. 3. London: Technical Editing and Reproduction.

WILLMARTH, W. W. & BOGAR, T. J. 1977 *Phys. Fluids. Suppl.* **20**, S9.

WILLMARTH, W. W. & SHARMA, L. K. 1983 Study of turbulent structures with hot-wires smaller than the viscous lengthscale. Submitted to *J. Fluid Mech.*

ZAKKAY, V., BARRA, V. & HOZUMI, K. 1980 In *Turbulent Boundary Layers – Experiments, Theory & Modelling, AGARD* CP 271, p. 4. Technical Editing and Reproduction.

ZAKKAY, V., BARRA, V. & WANG, C. R. 1978 *AIAA J.* **17**, 356.